Lab on a Chip

Miniaturisation for chemistry, physics, biology, materials science and bioengineering

www.rsc.org/loc

Volume 11 | Number 22 | 21 November 2011 | Pages 3727–3922

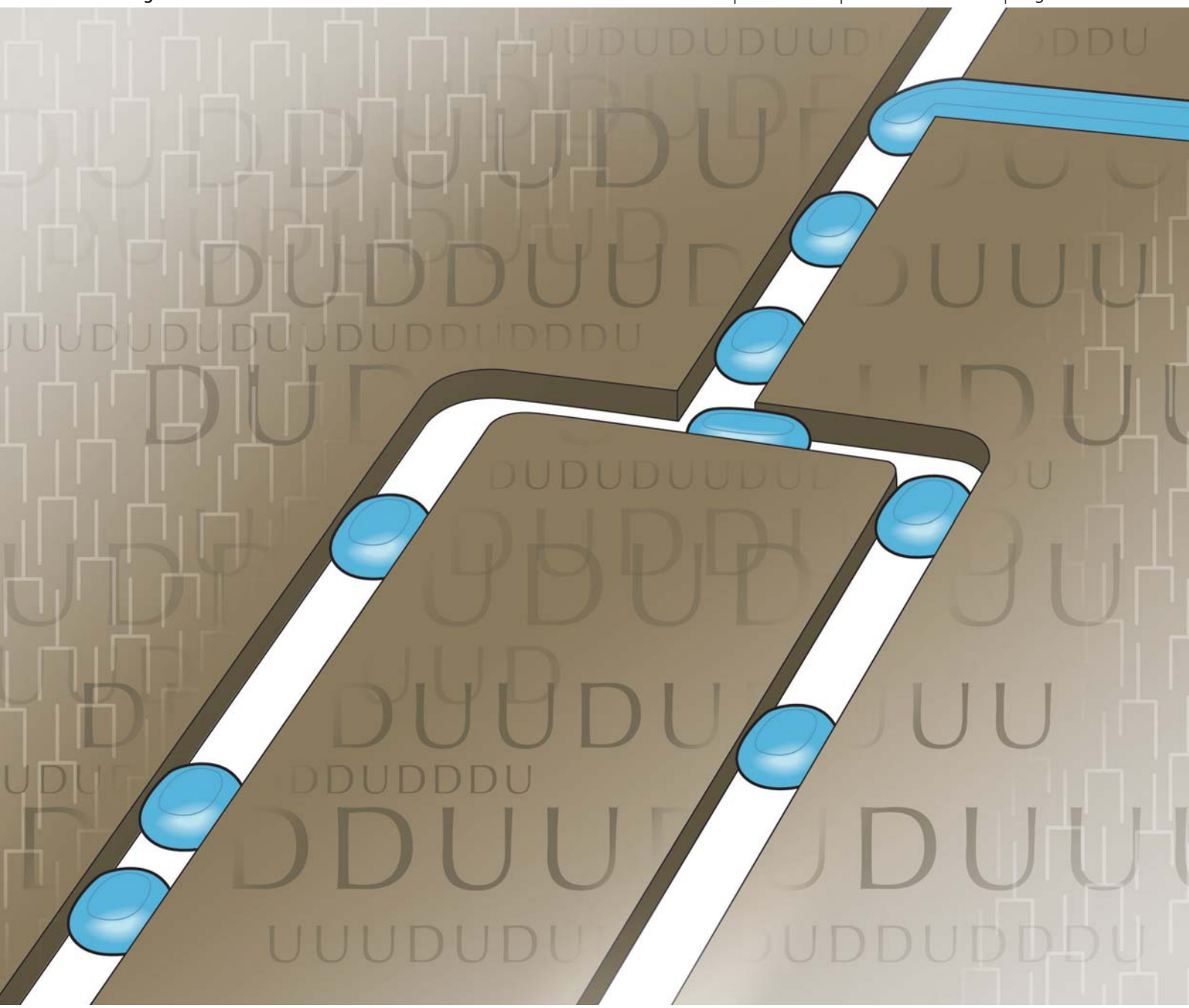

ISSN 1473-0197

RSC Publishing

PAPER

Ren *et al.*

Passive droplet trafficking at microfluidic junctions under geometric and flow asymmetries

Lab on a Chip

Dynamic Article Links

Cite this: *Lab Chip*, 2011, **11**, 3774

www.rsc.org/loc

PAPER

Passive droplet trafficking at microfluidic junctions under geometric and flow asymmetries†

Tomasz Glawdel, Caglar Elbuken and Carolyn Ren*

Received 13th July 2011, Accepted 19th August 2011
DOI: 10.1039/c1lc20628a

When droplets enter a junction they sort to the channel with the highest flow rate at that instant. Transport is regulated by a discrete time-delayed feedback that results in a highly periodic behavior where specific patterns can continue to cycle indefinitely. Between these highly ordered regimes are chaotic structures where no pattern is evident. Here we develop a model that describes droplet sorting under various asymmetries: branch geometry (length, cross-section), droplet resistance and pressures. First, a model is developed based on the continuum assumption and then, with the assistance of numerical simulations, a discrete model is derived to predict the length and composition of the sorting pattern. Furthermore we derive all unique sequences that are possible for a given distribution and develop a preliminary estimation of why chaotic regimes form. The model is validated by comparing it to numerical simulations and results from microfluidic experiments in PDMS chips with good agreement.

1. Introduction

We study the trafficking of droplets using both numerical and experimental techniques at a simple T-junction under asymmetries in geometry (channel length, cross-section) and flow (exit pressure, droplet resistance). With the assistance of numerical simulations of the idealized system a discrete model is derived that predicts the pattern length, distribution of droplets between the two branches, and bifurcations between consecutive regimes. We then restrict the model to studying the more practical situation of only asymmetric branch lengths and pressures, where pressures can be used to control the distribution of droplets in the two branches by biasing the flow. In addition, we derive all unique sequences that are possible for a given distribution and develop a preliminary estimation of whether sorting will be ordered or chaotic. The model is validated against numerical simulations that represent the physical system and results from microfluidic experiments in PDMS based chips. Finally, we present insights on how to effectively design a "*random droplet sampler*" for dividing a population of droplets into two groups.

Once droplets are generated they travel along a series of conduits that compose the microfluidic network. For the trivial case of one exit, droplets simply move along at a fixed speed and spacing under a given set of conditions. However, when junctions are added, droplets can choose more than one path, and the transport of droplets increases in complexity. The increasing complexity lies in the fact that droplets alter the hydrodynamic resistance of the channel they travel within which influences the global flow field. This creates a feedback effect, whereby the decision made by a preceding droplet influences the decision of subsequent droplets that enter a bifurcation. In some cases, the sequence of decisions can form a pattern of droplet trajectories that repeats indefinitely; while under other circumstances the system is chaotic.[1–3]

Droplet trafficking is thus an example of the transport of discrete elements, or signals, through networks consisting of nodes that impart a non-linear behaviour,[4–6] analogous to transport of cars on roads,[7] blood cells through capillaries[8] and neural networks.[9] The long-distance interaction between droplets through the global flow field has been exploited to create interactive elements such as logic gates,[10,11] signal encoder/decoders,[12,13] sorters,[1,14,15] and automated coalescence[16] and storage units.[17] Understanding the motion of droplets in networks is critical to the development of droplet microfluidics; particularly, for combinatorial studies involving multiple reagents and conditions, where achieving high throughput through multiplexing and massive parallelization will require effective trafficking of droplets to their intended destinations.[18–20]

2. Conceptual framework

Droplets that enter a junction may either split into two daughter droplets, or sort into one of the outlet channels depending on the size of the droplet and the flow conditions.[21] The mechanism that governs sorting differs depending on the size of the droplets relative to the channel, which may be classified into three

Department of Mechanical and Mechatronics Engineering, University of Waterloo, 200 University Ave W., Waterloo, ON, Canada N2L 3G1. E-mail: c3ren@mecheng1.uwaterloo.ca; Fax: +1 519 888-4567; Tel: +1 519 888-4567 extn: 33030

† Electronic supplementary information (ESI) available. See DOI: 10.1039/c1lc20628a

sub-regimes: external flow mediated, collision mediated and feedback mediated. In external flow mediated sorting, droplets are simply travelers that do not alter the flow field significantly and ride along the streamlines that divide into the two outlets.[22] Droplets are much smaller than the size of the channel and are spaced far apart so they do not interact. If conditions remain the same, but the spacing is reduced, droplets may collide at the junction when they become stagnated leading to a new regime of collision mediated sorting.[23] Feedback mediated sorting covers the remaining conditions between collision/external flow mediated sorting and splitting, and is the focus of this study. In this regime, sorting at the junction is governed by a simple rule: droplets always sort into the branch with the highest flow rate[24] in order to balance the distribution of flow to the two outlets.

There are two operational modes for the junction: filtering or sorting (also termed repartition).[24–26] Filtering occurs when all the droplets sort into only one of the branches. This occurs at high dilution when the population of droplets in the filtering branch is insufficient to balance the two flow rates. At lower dilutions droplets divide between the two outlets. The transition between the two modes is defined by a critical spacing, λ_f, which may also be interpreted as a critical number of droplets that increase the resistance of the smaller channel to match that of the larger channel.

As droplets begin to sort, fascinating sorting patterns can form. For example, defining a droplet as going into Branch #1 as up and Branch #2 as down symbolized by ↑U and ↓D, respectively, a sequence such as UDUUDUD can form. Once set in place, sequences are generally stable being able to withstand most natural disturbances. Large disturbances can cause the specific pattern to change (*i.e.* UDUUDUD to UUUDDUD) but the overall pattern length and composition remain the same.[1] Hence the system is often said to exhibit "memory". Initial conditions influence the specific sequence which forms, but have no effect on the pattern length once steady state is reached.[1,2]

Once a droplet makes a decision at a junction it influences other droplets over the time period that it remains in the channel. Therefore, each decision has a finite lifespan, or time-delay for which it remains active. Hence cyclic periods correspond to the residence times of droplets in the branches.[2] Parametric studies have shown that the length and composition of the pattern depend on the incoming spacing compared to the channel lengths, and the droplet resistance to the channel resistance.[1–3,26] Pattern complexity increases as the incoming spacing decreases since more droplets are present in the channel. Surrounding the islands of periodic order are regimes where the system is chaotic, yet the droplets still divide in proportions that minimize the flow imbalance.

Previously reported studies mainly focused on differences in branch lengths as the only asymmetry in the junction. In reality, any asymmetry can cause a flow imbalance and thus affect the sorting behaviour. Therefore, it is important to investigate the effects of asymmetries in geometry including both branch lengths and cross-sectional areas, droplet (resistances) and flow conditions (outlet pressures). Geometric asymmetries can be imposed by the design and fabrication of the network. Changes in the cross-sectional area have a dual effect. First, the relative speed of the droplets changes between the two channels, and second, the resistance changes in a non-linear manner for both the channel and droplet.[4–6] Droplet resistances in both branches may vary based on the geometry, or by external influences such as heating one branch to change the viscosity.[27] Adjusting the outlet pressures changes the flow rates to the two branches and is thus a simple means of regulating the distribution of droplets in the channels. A pressure imbalance can also occur naturally. For example, if the exits of the sorter are connected to a larger network, then changing flow conditions downstream can alter the pressures at the exits. These examples encompass all the asymmetries that are probable at a microfluidic junction.

To aid in the understanding of the sorting problem we use a numerical scheme that mimics the real physical system. From observations of the numerical experiments, a model based on the continuum approximation is developed followed by a discrete model that predicts the periodic behaviour. In addition to predicting the pattern length, composition and bifurcations, the model also includes a stability analysis to determine whether a predicted pattern will revert to chaos. A method for determining all of the unique sequences that can occur for a given pattern composition is also presented. Finally, the predictive power of the model is quantified by comparing it to both numerical and experimental results.

3. Numerical simulations

Numerical simulations can help to fill the knowledge gap by providing an idealized set of experimental data that makes the problem more manageable. The algorithm developed for this study builds upon the work of Jousse *et al.*,[26] Schindler and Ajdari,[28] Smith and Gaver,[3] Sessoms *et al.*,[2,25] Cybulski and Garstecki[1] and Behzad *et al.*[12] These works take the approach that droplets can be treated as point particles and microchannels can be reduced to 1-D pipe networks. In this work we develop two types of simulations. The first mimics the real system where flow rates are allowed to oscillate naturally (full model), and the second mimics the idealized process by setting the flow rates to be equal (ideal model). The later provides valuable information that is used to develop the discrete sorting model.

3.1 Model domain and description

Relevant variables describing the operation of the T-junction sorter are presented in Fig. 1. Droplets enter the system from the main channel with an incoming spacing (λ) and frequency (f) and

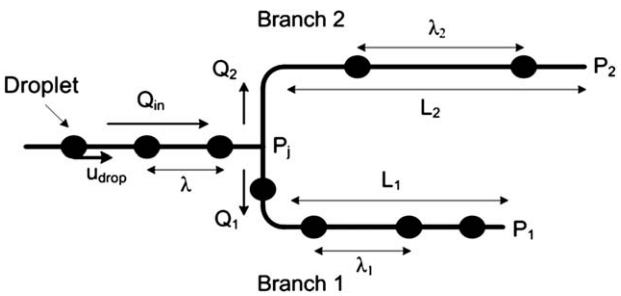

Fig. 1 Schematic of the junction where droplet sorting occurs with all relevant variables identified. Asymmetry may exist in the branch lengths, cross-sections, droplet resistances and applied pressures.

leave with spacings λ_1, λ_2 and frequencies f_1, f_2. The system is defined by two outlet branches with lengths L_1, L_2, base hydrodynamic resistances $R^{(1)}_{hyd}$, $R^{(2)}_{hyd}$, cross-sections w_1h_1, w_2h_2 and applied exit pressures P_1, P_2. Each channel may also have a unique droplet resistance ($R^{(1)}_{drop}$, $R^{(2)}_{drop}$). Because of decisions at the junction, the number of droplets in the two branches (n_1, n_2) changes dynamically as droplets sort or exit the system which causes the two flow rates (Q_1, Q_2) to oscillate.

3.2 Full-model simulations

Droplets travel along the branches of the network with a slip factor β (relative speed of the droplets to the average speed of flow), and hydrodynamic resistance R_{drop}. These two terms are assumed to be constant in the channel, thus any capillary number Ca or spacing dependence is omitted from this model.[4–6] We also omit other non-idealities that are present in the real physical system including the finite size of the droplets, stagnation of the droplets at the junction before they sort, and conditions where splitting[21,29,30] or collisions[23] may occur. Formation, sorting and associated events occur instantaneously without delay. When a droplet enters the bifurcation it always chooses the branch with the highest instantaneous flow rate.

A highly variable explicit time stepping scheme is used to calculate the droplet distribution within the network.[24,28] The new time step is calculated by determining the shortest interval for one of three events to occur that may change the droplet distribution: (1) a new droplet is generated, (2) a droplet reaches the junction and needs to be sorted, and (3) a droplet exits one of the two branch channels. At each time step the total flow rates are calculated by applying compact modelling methods.[31] This leads to a system of equations that describe the flow rates in each channel, Q_{1-3}, and internal pressure at the junction P_1, from the instantaneous resistance of the channels R_{1-3}. The hydrodynamic resistance of a rectangular microchannel is a non-linear function that scales as L/wh^3.[31] Droplet velocities are calculated as: $u_{di} = Q_i\beta_i/A_i$, where Q_i is the flow rate and A_i the cross-sectional area. Subsequently, the time step is calculated as the minimal interval to the next event. This time step is then used to convect each droplet in the network according to their local velocity ($\Delta x_i = u_{di}\Delta t$). If a new droplet is formed it is added to the beginning of the inlet channel. If a sorting event occurs, a droplet is added to the appropriate channel and removed from the incoming channel. If a droplet leaves one of the two outlets it is simply removed from that channel.

Simulations begin with no droplets present in the network. For each configuration (geometry, pressures, *etc.*) droplets are generated over a wide range of frequencies to obtain different incoming spacings. For each frequency setting, the sorting of at least 1000 droplets is recorded to ensure that the system reaches a steady state. The sequence of decisions is recorded as a string (*i.e.* UUDUDUD…), and a template-matching algorithm is used to detect a repeating pattern if it exists.[3]

3.3 Ideal-model simulations

Developing a theoretical model based on the numerical results is an arduous task given the non-linear coupling between the number of droplets in the channel, the flow rates and the sorting rule. To make the problem more manageable, we follow the strategy taken by Sessoms *et al.* and develop an idealized numerical simulation of the trafficking problem.[2] The difference is that in the full-model simulations the flow rates in the branches are allowed to oscillate, while in the ideal-model the flow rates in the branch channels are constant and always equal to one half the incoming flow rate ($Q_{1,2} = Q/2$). Since the flow rates are fixed, the time step is also fixed at λ, and the spacing of the droplets in the branches are constant and equal to multiples of $\lambda/2$. Thus only a finite number of droplet distributions exist, the system is completely deterministic, and a periodic behaviour is expected for all incoming spacings.

Droplets sort in order to balance the flow between the two branches. When a droplet enters the bifurcation it chooses the branch with the highest flow rate at that moment, which is captured by the following function ψ_t that defines the expected difference in flow ($Q_1 - Q_2$):

$$\psi_t = \frac{R^{(1)}_{hyd}}{R^{(1)}_{drop}}\left[\frac{P_j - P_1}{P_j - P_2}\left(\frac{R^{(2)}_{hyd}}{R^{(1)}_{hyd}}\right) - 1\right] + \frac{R^{(2)}_{drop}}{R^{(1)}_{drop}}\left(\frac{P_j - P_1}{P_j - P_2}\right)N_2 - N_1 \quad (1)$$

A positive value of ψ_t results in a droplet flowing into Branch #1 and a negative into Branch #2. In addition to tracking the droplets through the network, we also track the "holes" left behind by a droplet after it makes a decision. Every sorting event thus simultaneously creates a droplet that sorts into the appropriate channel as well as a "hole" that sorts into the other channel. By analyzing the number of droplets (N_1, N_2) and holes (N_{H1}, N_{H2}) present in each channel, Sessoms *et al.* were able to derive a set of selection rules that determines the length of the emerging pattern.[2] In the development of a discrete model we also take this approach. A video of sorting from the ideal-model simulations is available in the ESI†.

4. Predictive model

In this section, two complementary analytical models are developed; the first treats the droplets as a continuous medium and the second as discrete elements. The goal of the predictive model is to capture all of the salient features of the sorting process. This includes the identification of transitions (i) between filtering and sorting, (ii) between periodic and chaotic regimes, (iii) distribution of droplets between the two outlets, and (iv) the length and composition of the periodic sequence.

Similar continuum models have been developed for loop structures and asymmetric bifurcations by Sessoms *et al.*, Cybulski and Garstecki, and Engl *et al.* to obtain mean field approximations of droplet trafficking.[1,24,25] Here these works are adapted, and improved, to account for all probable types of asymmetries. As well, droplet spacing[25] rather than frequency[1] was chosen as the parameter characterizing sorting, since the former leads to a less ambiguous set of equations that are easier to interpret. A model is first developed for the general case (all asymmetries), which is then simplified to study the more practical circumstance of only asymmetric branch lengths and pressures. Using the continuum model combined with observations from the ideal-model simulations a discrete model is developed to

predict the periodic behaviour of the system. Note that in the following derivation dimensionless values are marked by an asterisk.

4.1 Continuum model: general case

The first task is to determine which of the two branches the droplets filter into first, followed by the critical point where droplets stop filtering and begin sorting into both channels. By default the shorter channel is not necessarily the filtering channel since a pressure bias can cause it to have a larger effective resistance. The filtering channel is actually the one with the naturally higher flow rate in the absence of droplets, which can be determined by taking a ratio of the flow rates:

$$\frac{Q_1}{Q_2} = \frac{P_j - P_1}{R_{\mathrm{hyd}}^{(1)}} \frac{R_{\mathrm{hyd}}^{(2)}}{P_j - P_2} = \frac{R_{\mathrm{eff}}^{(2)}}{R_{\mathrm{eff}}^{(1)}} \tag{2}$$

Envisioning that the same pressure drop ($P_j - P_1$) was applied across both branches, an effective resistance can be defined that accounts for the pressure imbalance: $R_{\mathrm{eff}}^{(1)} = R_{\mathrm{hyd}}^{(1)}$, $R_{\mathrm{eff}}^{(2)} = R_{\mathrm{hyd}}^{(2)}/P^*$, where P^* is defined as the non-dimensional pressure skew between the two outlets. If $R_{\mathrm{eff}}^{(2)}/R_{\mathrm{eff}}^{(1)} \geq 1$, then Branch #1 is the filtering channel, and if not it is Branch #2. From this point onwards, the filtering channel is designated with the subscript a and the sorting channel with b. P^* is recalculated as $P^* = (P_j - P_{\mathrm{b}})/(P_j - P_{\mathrm{a}})$ and the effective lengths, hydrodynamic resistances, cross-sections, and droplet resistances are re-designated as well.

Droplets choose the channel with the highest flow rate when they enter the junction; this naturally forces the total flow rates ($Q_{\mathrm{T}}^{(\mathrm{a})}$, $Q_{\mathrm{T}}^{(\mathrm{b})}$) to be nearly equal over the long term in the sorting regime.[3,24,25,28] Applying conservation of mass to the dispersed phase: $Q_{\mathrm{d}} = Q_{\mathrm{d}}^{(\mathrm{a})} + Q_{\mathrm{d}}^{(\mathrm{b})}$, where $Q_{\mathrm{d}} = V_{\mathrm{d}} f$, V_{d} is the droplet volume and f the frequency. Substitution reduces the previous equation to: $f_{\mathrm{d}} = f_{\mathrm{d}}^{(\mathrm{a})} + f_{\mathrm{d}}^{(\mathrm{b})}$. Frequency is related to the droplet speed and average spacing by $f = u_{\mathrm{drop}}/\lambda$. Droplets move at a slip relative to the average velocity of the total flow rate in the channel. Assuming that the incoming flow rate splits *equally* between the two channels:

$$\frac{2\beta_{\mathrm{in}}}{A_{\mathrm{in}}\lambda} = \frac{\beta_{\mathrm{a}}}{A_{\mathrm{a}}\lambda_{\mathrm{a}}} + \frac{\beta_{\mathrm{b}}}{A_{\mathrm{b}}\lambda_{\mathrm{b}}} \tag{3}$$

where the subscript 'in' refers to the incoming channel that leads to the T-junction, A is the cross-sectional area and β the slip. Spacing is related to the number of droplets in each branch by $n = L/\lambda$, resulting in the following equation:

$$\frac{2\beta_{\mathrm{in}}}{A_{\mathrm{in}}\lambda} = \left(n_{\mathrm{a}} \frac{\beta_{\mathrm{a}}}{A_{\mathrm{a}}L_{\mathrm{a}}} + n_{\mathrm{b}} \frac{\beta_{\mathrm{b}}}{A_{\mathrm{b}}L_{\mathrm{b}}} \right) \tag{4}$$

Filtering occurs when all of the incoming droplets pass through Branch a. Therefore, applying the spacing relationship, $\lambda_{\mathrm{a}} = \lambda/2$, for perfectly divided flow rates, and setting $n_{\mathrm{b}} = 0$, the critical value where droplets begin to sort is:

$$\frac{2}{\lambda_f^*} \geq \frac{\left(R_{\mathrm{hyd}}^* - P^*\right)}{P^* R_{\mathrm{drop}}^{*(\mathrm{a})}} \tag{5}$$

where the various non-dimensional factors will be defined later.

Using compact modelling of the flow, the flow rate in each branch is:

$$Q^{(\mathrm{a})} = \frac{P_j - P_{\mathrm{a}}}{R_{\mathrm{hyd}}^{(\mathrm{a})} + n_{\mathrm{a}} R_{\mathrm{drop}}^{(\mathrm{a})}}; \quad Q^{(\mathrm{b})} = \frac{P_j - P_{\mathrm{b}}}{R_{\mathrm{hyd}}^{(\mathrm{b})} + n_{\mathrm{b}} R_{\mathrm{drop}}^{(\mathrm{b})}} \tag{6}$$

where now the total hydrodynamic resistance of the channels is the sum of the base resistance and the resistance added by the droplets. Droplet resistance may also be defined as an equivalent added channel length $L_{\mathrm{drop}} = R_{\mathrm{drop}} L/R_{\mathrm{hyd}}$.[4] On average the two flow rates are equal to each other, $Q_{\mathrm{d}}^{(\mathrm{a})} = Q_{\mathrm{d}}^{(\mathrm{b})}$, and by substituting eqn (4) and (6) a solution for n_{a} and n_{b} can be found:

$$n_{\mathrm{a}} = \frac{1}{\left(\Lambda^* + \dfrac{P^*\beta^*}{R_{\mathrm{drop}}^* A^*}\right)} \left(\frac{2}{\lambda^*} \frac{\Lambda^* A^{*(\mathrm{a})}}{\beta^{*(\mathrm{a})}} + \frac{\beta^*}{R_{\mathrm{drop}}^{*(\mathrm{a})} R_{\mathrm{drop}}^* A^*} \left(R_{\mathrm{hyd}}^* - P^* \right) \right)$$

$$n_{\mathrm{b}} = \frac{\dfrac{P^*}{R_{\mathrm{drop}}^*}}{\left(\Lambda^* + \dfrac{P^*\beta^*}{R_{\mathrm{drop}}^* A^*}\right)} \left(\frac{2}{\lambda^*} \frac{\Lambda^* A^{*(\mathrm{a})}}{\beta^{*(\mathrm{a})}} - \frac{\Lambda^*}{R_{\mathrm{drop}}^{*(\mathrm{a})} P^*} \left(R_{\mathrm{hyd}}^* - P^* \right) \right) \tag{7}$$

The total number of droplets in the two channels is $n_{\mathrm{T}} = n_{\mathrm{a}} + n_{\mathrm{b}}$:

$$n_{\mathrm{T}} = \frac{2}{\lambda^*} \frac{\Lambda^* A^{*(\mathrm{a})}}{\beta^{*(\mathrm{a})}} \frac{\left(1 + \dfrac{P^*}{R_{\mathrm{drop}}^*}\right)}{\left(\Lambda^* + \dfrac{P^*\beta^*}{R_{\mathrm{drop}}^* A^*}\right)} - \frac{\left(R_{\mathrm{hyd}}^* - P^*\right)}{R_{\mathrm{drop}}^{*(\mathrm{a})} R_{\mathrm{drop}}^* A^*} \frac{\left(\Lambda^* A^* - \beta^*\right)}{\left(\Lambda^* + \dfrac{P^*\beta^*}{R_{\mathrm{drop}}^* A^*}\right)} \tag{8}$$

where the various non-dimensional factors are summarized as:

$$\lambda^* = \frac{\lambda}{L_{\mathrm{a}}}, \ \Lambda^* = \frac{L_{\mathrm{b}}}{L_{\mathrm{a}}}, \ A^{*(\mathrm{a})} = \frac{A_{\mathrm{a}}}{A_{\mathrm{in}}}, \ A^* = \frac{A_{\mathrm{b}}}{A_{\mathrm{a}}}, \ \beta^{*(\mathrm{a})} = \frac{\beta_{\mathrm{a}}}{\beta_{\mathrm{in}}}, \ \beta^* = \frac{\beta_{\mathrm{b}}}{\beta_{\mathrm{a}}}$$

$$R_{\mathrm{drop}}^* = \frac{R_{\mathrm{drop}}^{(\mathrm{b})}}{R_{\mathrm{drop}}^{(\mathrm{a})}} R_{\mathrm{drop}}^{*(\mathrm{a})} = \frac{R_{\mathrm{drop}}^{(\mathrm{a})}}{R_{\mathrm{hyd}}^{(\mathrm{a})}} R_{\mathrm{hyd}}^* = \frac{R_{\mathrm{hyd}}^{(\mathrm{b})}}{R_{\mathrm{hyd}}^{(\mathrm{a})}}$$

Eqn (8) illustrates that the total number of droplets is a linear function of $2/\lambda^*$ and the rest of the variables define the slope and intercept. The frequency of droplets entering a channel is related by, $\beta_{\mathrm{a}} A_{\mathrm{a}} \lambda_{\mathrm{a}} f_{\mathrm{a}} = \beta_{\mathrm{in}} A_{\mathrm{in}} \lambda f/2$, which can then be used to find the probability of a droplet selecting a branch:

$$\mathrm{Prob}_{\mathrm{a}} = \frac{f_{\mathrm{a}}}{f} = \frac{n_{\mathrm{a}} \beta^{*(\mathrm{a})}}{\left(\dfrac{2}{\lambda^*}\right) A^{*(\mathrm{a})}}$$
$$\mathrm{Prob}_{\mathrm{b}} = 1 - \mathrm{Prob}_{\mathrm{a}} \tag{9}$$

Analysis by Sessoms *et al.* showed that the residence time in the two channels governs the sorting cycle.[2,25] Given that the

residence time is $t = L/u_{drop}$, and that the flow splits equally, the dimensionless periods for the two branches may be calculated as:

$$t_a^* = t_a f = \left(\frac{2}{\lambda^*}\right)\frac{A^{*(a)}}{\beta^{*(a)}}; \quad t_b^* = t_b f = \left(\frac{2}{\lambda^*}\right)\frac{\Lambda^* A^{*(a)} A^*}{\beta^{*(a)}\beta^*} \tag{10}$$

Again the term $2/\lambda^*$ appears as the governing parameter. Reconsidering the previous equations for n_a, n_b and n_T, they may be interpreted as being functions of the dimensionless period.

4.2 Continuum model: simplified case

In the simplified model the only asymmetry between the channels is the applied pressures and the branch lengths. Under these conditions several terms drop out: $A^{*(a)} = 1$, $A^* = 1$, $\beta^{*(a)} = 1$, $\beta^* = 1$, $R^*_{drop} = 1$ and $R^*_{hyd} = \Lambda^*$. The reconstituted equations become:

$$\begin{aligned} n_a &= \frac{1}{(\Lambda^* + P^*)}\left(\frac{2}{\lambda^*}\Lambda^* + \frac{1}{R^{*(a)}_{drop}}(\Lambda^* - P^*)\right) \\ n_b &= \frac{P^*}{(\Lambda^* + P^*)}\left(\frac{2}{\lambda^*}\Lambda^* - \frac{1}{R^{*(a)}_{drop}}\frac{\Lambda^*}{P^*}(\Lambda^* - P^*)\right) \\ n_T &= \frac{2}{\lambda^*}\Lambda^*\frac{(1+P^*)}{(\Lambda^* + P^*)} - \frac{(\Lambda^* - P^*)}{(\Lambda^* + P^*)}\frac{(\Lambda^* - 1)}{R^{*(a)}_{drop}} \end{aligned} \tag{11}$$

The new probabilities are: $Prob_a = n_a/(2/\lambda^*)$, $Prob_b = 1 - Prob_a$, and dimensionless residence times: $t_a^* = 2/\lambda^*$, $t_b^* = \Lambda^* 2/\lambda^*$.

Recall that the basis of the model assumes a continuous medium of droplets, in reality droplets are discrete elements which is the source of the periodic behaviour of the system. The continuum model does not provide a method of determining what pattern will form, or when a pattern will transition into a new one, yet it is still very useful as it provides information on the relationship between various factors on the distribution of droplets, and provides a foundation for the development of a discrete model that can be used to predict the periodic behaviour.

5. Discrete model

Extensive experiments were performed to understand the sorting process using the ideal-model numerical simulations in a similar manner to the work of Sessoms *et al.* and their study of sorting in asymmetric junctions.[2] From these observations a set of "selection rules" were developed that determine the sequence length and composition. The following discussion provides derivation of the rules for the simplified case; corresponding solutions for the general case are provided in the ESI†.

Transitions from one periodic regime to another depend on changes to the incoming spacing $2/\lambda^*$. The first transition occurs when the system switches from filtering to sorting. This occurs when the resistance of the filter branch becomes larger than the sorting branch (refer to eqn (5)). By accounting for the discrete nature of the system this occurs at:

$$\frac{2}{\lambda_f^*} = \text{floor}\left[\frac{(\Lambda^* - P^*)}{P^* R^{*(a)}_{drop}}\right] + 1 \tag{12}$$

where we define the number of droplets in Branch a needed to balance the two channels as: $N_{bal} = 2/\lambda_f^* - 1$. From this point forward capitalized N refers to droplet counts in the discrete model and small n for the continuum model. By increasing $2/\lambda^*$ further (decreasing the incoming spacing) droplets begin to sort into both branches. Based on the discretization of position, droplets in each channel now have a fixed retention time given by: $T_a^* = \text{ceil}(2/\lambda^*)$, $T_b^* = \text{ceil}(\Lambda^* 2/\lambda^*)$. Sessoms *et al.* showed that subsequent transitions in the periodic sequence occur when the discrete residence times (T_a^*, T_b^*) change values.[2]

This happens for specific spacings, $2/\lambda_c^*(k)$:

$$\frac{2}{\lambda_c^*(k)} = N_{bal} + k, \quad \frac{2}{\lambda_c^*(k)} = \frac{1}{\Lambda^*}(N_{bal} + k) \tag{13}$$

where $k \in N^*$. These critical spacings bracket regions where the pattern length remains the same and is equivalent to one of the residence times. Crossing from one region into another means that the cycle time of one of the branches is different, and thus the pattern may change.

Sessoms *et al.* developed a set of selection rules that define when the cycle time will equate to either T_a^* or T_b^* for the case of asymmetric channel lengths.[2] Through observation of the ideal-model simulations the authors found that the number of droplets and holes in the two branches are either both constant, or constant in one channel and varying by 1 in the other. They found an intriguing relationship between the two channels which allowed them to develop the sorting rules:

$$N_b + N_{Ha} = T_a^* - N_{bal},\ T_a^* - N_{bal} - 1 \tag{14}$$

In fact, this relationship can be derived from the sorting rule (eqn (1)) used in the ideal model. At first attempts were made to modify the approach taken by Sessoms *et al.* and adapt it to the general case without success.[2] The reason is that the addition of pressure bias and droplet resistance difference creates an unequal weighting in the influence a single droplet has on the flow rate in each channel. When a droplet enters Branch b it may require more than one droplet in Branch a to rebalance the flow. Thus the number of droplets may fluctuate by more than 1 to compensate for the unequal weighting. Due to this fact, a consistent relationship like the one in eqn (14) was not observed. Instead a new approach was taken to develop the "selection rules" using the continuum model as a basis.

Comparisons with numerical results indicated that the continuum model is able to predict the total number of droplets in the two branches quite accurately (data not shown). The formulation of n_T naturally includes all of the constraints in the model and is therefore the best description of the overall conditions. Using this as a basis, a modified equation is developed that includes the discrete nature of the system and mimics the conditions set forth in the ideal-model numerical simulations. Replacing $\Lambda^*_{dis} = T_b^*/T_a^*$ and $2/\lambda^* = T_a^*$, in eqn (11), the new discrete calculation for the total number of droplets becomes:

$$N_T = \text{ceil}\left[T_a^* \Lambda^*_{dis}\frac{(1+P^*)}{(\Lambda^* + P^*)} - \frac{(\Lambda^* - P^*)}{(\Lambda^* + P^*)}\frac{(\Lambda^* - 1)}{R^{*(a)}_{drop}}\right] \tag{15}$$

From the sorting rule (eqn (1)), and the relation given in eqn (15), a base value for N_b can be estimated:

$$N_b = \text{ceil}\left[\frac{P^*}{P^* + R^*_{drop}}\left(N_T - \frac{(\Lambda^*_{dis} - P^*)}{P^* R^{*(a)}_{drop}}\right)\right] \quad (16)$$

and by extension $N_a = N_T - N_b$, and $N_{Ha} = T^*_a - N_a$, and $N_{Hb} = T^*_b - N_b$. Observations show that $N_a + N_b$ can only take on certain values: (i) N_a and N_b are both constant and the cycle is a harmonic $T^*_{cyc} = |T^*_a - T^*_b|$, (ii) N_a is constant and N_b fluctuates by 1, ($N_a + N_b = N_T, N_T - 1$), $T^*_{cyc} = T^*_a$, (iii) N_b is constant and N_a fluctuates by 1 and ($N_a + N_b = N_T, N_T - 1$), $T^*_{cyc} = T^*_b$ and (iv) N_b is constant and N_a fluctuates by more than 1 ($N_a + N_b = N_T, N_T - 1, N_T + 1$), $T^*_{cyc} = T^*_b$. Only one of the four possible cases can occur. To determine which one does, a series of tests are applied to confirm that the conditions satisfy (a) oscillations around the zero point and (b) conservation of the total number of droplets in the two branches over the cycle time. Therefore, four separate scenarios can occur for the sorting function ψ:

$$\begin{aligned}
\psi_1 &= \frac{R^*_{hyd} - P^*}{R^{*(a)}_{drop} P^*} + R^*_{drop}\frac{N_b}{P^*} - N_a \\
\psi_2 &= \frac{R^*_{hyd} - P^*}{R^{*(a)}_{drop} P^*} + R^*_{drop}\frac{N_b - 1}{P^*} - N_a \\
\psi_3 &= \frac{R^*_{hyd} - P^*}{R^{*(a)}_{drop} P^*} + R^*_{drop}\frac{N_b - 1}{P^*} - N_a - 1 \\
\psi_4 &= \frac{R^*_{hyd} - P^*}{R^{*(a)}_{drop} P^*} + R^*_{drop}\frac{N_b}{P^*} - N_a - 1
\end{aligned} \quad (17)$$

For test (a) to be satisfied ψ must switch between positive and negative values. Omitting case (i) for the moment, then a criteria for the three other cases (ii–iv) can be calculated through a series of ratios of ψ_{1-4}: case (ii) $Ch_1 = \psi_1/\psi_2$, (iii) $Ch_2 = \psi_2/\psi_3$, and (iv) $Ch_3 = \psi_1/\psi_4$. A case is possible if the respective ratio ≤ 0 indicating that the sorting function switches signs. If a case passes the first test then the second test is to verify that it can be fulfilled within the expected cycle time. Over the cycle the total number of holes and droplets must be conserved, for case (ii) $(T_a - t)N_b + t(N_b - 1) = T_b N_{Ha}$ and case (iii), $(T_b - t)N_a + t(N_a + 1) = T_a(N_{Hb} + 1)$, leading to the following conditions for t:

$$\text{(ii)}\ 0 < n_b - \frac{T_b}{T_a} n_{Ha} < 1, \quad \text{(iii)}\ 0 < \frac{T_a}{T_b}(n_{Hb} + 1) - n_a < 1 \quad (18)$$

If either condition equates to 0 or 1 then case (i) is active as the total number of droplets is constant. If the cycle time condition is not satisfied for (ii) then the only option left is the more complex case (iv).

From this information the composition of the actual pattern can be determined. The total length of the pattern is given by $|\Omega| = T^*_{cyc}$, and the number of Ds and Us in the pattern for the four cases are:

$$\text{(i)}\ N_D = N_{Ha},\ N_U = T^*_{cyc} - N_D$$

$$\text{(ii)}\ N_D = N_{Ha},\ N_U = T^*_{cyc} - N_D$$

$$\text{(iii)}\ N_D = N_b - 1,\ N_U = T^*_{cyc} - N_D \quad \text{(iv)}\ N_D = N_b\ N_U = T^*_{cyc} - N_D.$$

Finally, the probability of droplets sorting into each channel may be calculated: $\text{Prob}_a = N_U/|\Omega|$, $\text{Prob}_b = 1 - \text{Prob}_a$. For convenience, the "selection rule" algorithm is summarized in a flow chart available in the ESI†. The outcome, in terms of the number of droplets in each channel, expected pattern length and composition is summarized below in Table 1 for all possible cases.

5.1 Possible unique sequences

Once the pattern length and composition (N_U, N_D) are known, the number of possible sequences can be obtained from counting all permutations for the pattern length:[1]

$$|\Omega_{dis}| = \frac{T^*_{cyc}!}{N_U!\,N_D!} \quad (19)$$

However, this calculation does not eliminate redundant cyclic shifts that occur. For example, UUUUDD may be shifted as UUUDDU or UDDUUU and so on. For the case of 4 Us and 2 Ds there are 15 possible distributions, consisting of only 3 unique sequences: UUUUDD, UUUDUD, and UUDUUD. As the pattern length increases, determining the number of unique sequences, $|\Omega_{seq}|$, becomes progressively more difficult.

Fortunately, this type of problem can be solved using Póyla's counting method for cyclic groups.[32] In the ESI†, we provide an example of the methodology and summarize the specific sequences that can be obtained for pattern lengths $|\Omega_{seq}| = 2 \rightarrow 9$ with different compositions. A pattern length of $|\Omega_{seq}| = 9$, for instance, has 4 unique patterns with 2 Ds, 10 with 3 Ds and 14 with 4 Ds.

Although we can identify all the unique sequences that can form for a given set of Us and Ds, some may not be physically attainable. Cybulski and Garstecki noted that all possible sequences could usually be obtained; however, in certain narrow regions some sequences were absent.[1] They surmise that in the space of all possible initial configurations for the system the patterns may have different measures of their basins of attraction—some being of zero-order.

6. Results and discussion

First, an explanation of the general presentation of the results is required, as the same format is used throughout this section (refer to Fig. 2). Results are plotted *versus* the incoming droplet spacing $2/\lambda^*$, which was identified in the analytical modelling as the critical variable that defines the sorting phenomenon. All data from the numerical or experimental results are plotted using markers such as circles (○) or triangles (△). Predictions made by the discrete model are plotted using solid lines of various colours. The vertical dashed lines on the left side of the plot are the prediction for the limit of the filtering regime as calculated by the continuum (–) and discrete (·-) models. Alternating grey and white regions define the areas where the cycle time is expected to be the same as calculated by the bounds from eqn (13). Crossing from one region into another may cause the cycle time to change so we expect discontinuities to occur at these points.

Fig. 2 shows the pattern length and distribution of droplets for a prototypical result from the ideal-model simulations. The two black lines in Fig. 2a are the cycle times of the two branches

Table 1 List of outcomes from the discrete model for the selection rules. Calculations are with respect to the base value N_b from eqn (16)

Case	Condition	T^*_{cyc}	Branch A	Branch B	N_D
(i)	(ii) $t = 0$	$\lvert T^*_b - T^*_a \rvert$	N_a, N_{Ha}	N_b, N_{Hb}	N_{Ha}
	(ii) $t = 1$	$\lvert T^*_b - T^*_a \rvert$	N_a, N_{Ha}	$N_b - 1$, $N_{Hb} + 1$	N_{Ha}
	(iii) $t = 0$	$\lvert T^*_b - T^*_a \rvert$	N_a, N_{Ha}	$N_b - 1$, $N_{Hb} + 1$	$N_b - 1$
	(iii) $t = 1$	$\lvert T^*_b - T^*_a \rvert$	$N_a + 1$, $N_{Ha} - 1$	$N_b - 1$, $N_{Hb} + 1$	$N_b - 1$
(ii)	$0 < t < 1$	T^*_a	N_a, N_{Ha}	N_b, $N_b - 1$, N_{Hb}, $N_{Hb} + 1$	N_{Ha}
(iii)	$0 < t < 1$	T^*_b	N_a, $N_a + 1$, N_{Ha}, $N_{Ha} - 1$	$N_b - 1$, $N_{Hb} + 1$	$N_b - 1$
(iv)	(ii) $t < 0$, or $t > 1$	T^*_b	$N_a - 1$, $N_a + 1$, $N_{Ha} + 1$, $N_{Ha} - 1$	N_b, N_{Hb}	N_b

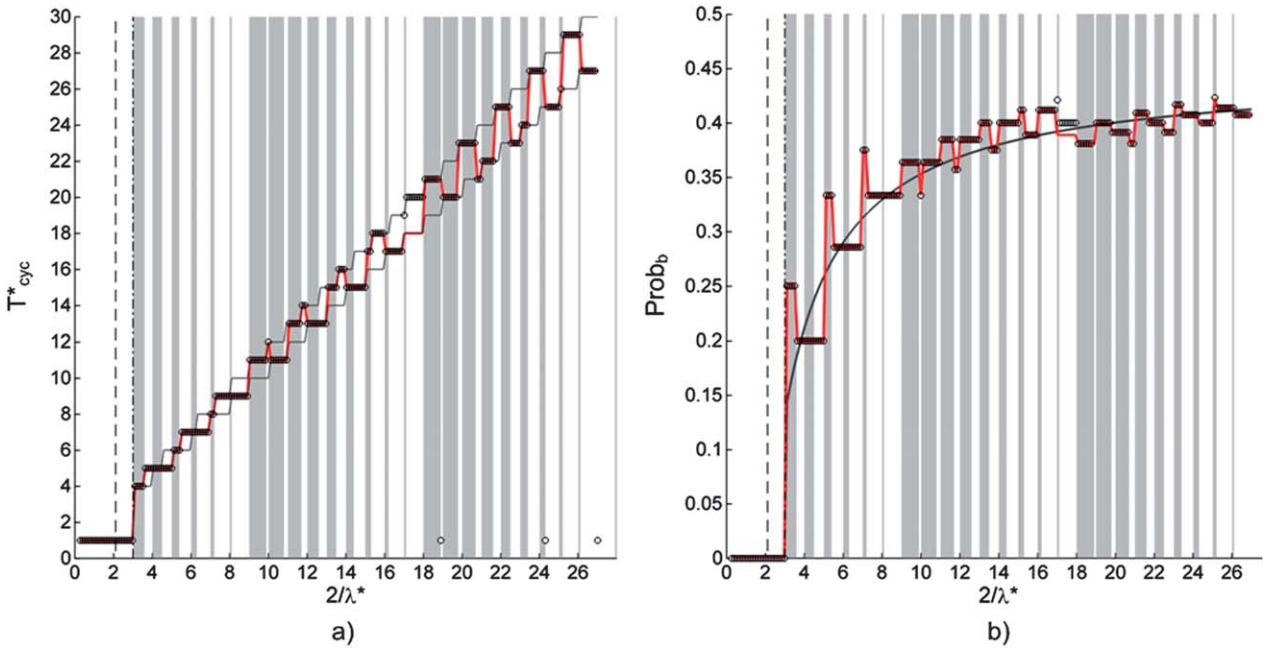

Fig. 2 Ideal-model numerical simulation results for (a) T^*_{cyc} and (b) P_b for $\Lambda^* = 0.8$, $P^* = 1$, $R^{*(a)}_{drop} = 0.1$. Red line is the prediction from the selection rules. Results where $T^*_{cyc} = 1$ are numerical artefacts caused by round-off errors near bifurcations.

(T_a^*, T_b^*) and the red line is the prediction made by the selection rule algorithm (T_{cyc}^*). As expected, the sorting system oscillates between the two potential cycle times in a non-trivial manner. The discrete model is able to accurately predict the limit of the filtering regime and shows a significant improvement over the continuum model prediction. In this example the number of droplets needed to balance the system $N_{bal} = 3$ in Branch a. As predicted, cycle times correspond either to T_a^* or T_b^* and transitions from one regime to another are accurately predicted by eqn (13). Within a region (white or grey) the pattern length remains the same but the specific cycle may be different. From the visual representation of the alternating grey and white regions, one can clearly see the striking complexity that can arise in the cyclic structure. In Fig. 2b the distribution of droplets is plotted ($Prob_b$) for the same case, where the red line is the prediction for the discrete model and the black for the continuum model. Additional comparisons for general and simplified cases are provided in the ESI†. We also tested the effect of initial conditions by randomly distributing droplets in the two branches at the start. Results were in agreement with the other works:[1,2] the overall pattern length remained the same but the specific sequence that appeared was different.

Recall that the only difference with the full-model case studies is that the flow rates are allowed to oscillate naturally. Although the discrete model does not consider these oscillations, all of the salient features are still captured when applied to the full-model studies, with the exception of additional chaotic regions appearing between two successive plateaus which can grow to the point where certain periodic regimes completely disappear.

Plots are in a similar format as before (refer to Fig. 3), except that when the simulation produces no discernible pattern or the pattern length is greater than twice the number of droplets in the channel then it is set to 0. These are the regions where the system is chaotic. As can be seen in Fig. 3a and c, these chaotic regimes are located near bifurcations from one plateau to another. The size of these regimes grows with increasing $2/\lambda^*$ until certain regions disappear. For instance, there are no even sequences above $T_{cyc}^* = 12$ for Fig. 3a, and no odd sequences above $T_{cyc}^* = 11$ for Fig. 3c. Even in the chaotic regimes the system still emulates the predictions put forth by the discrete model; however, as the density of droplets increases ($2/\lambda^*$ increases) the system moves towards the continuum model prediction as the limit of that assumption is approached.

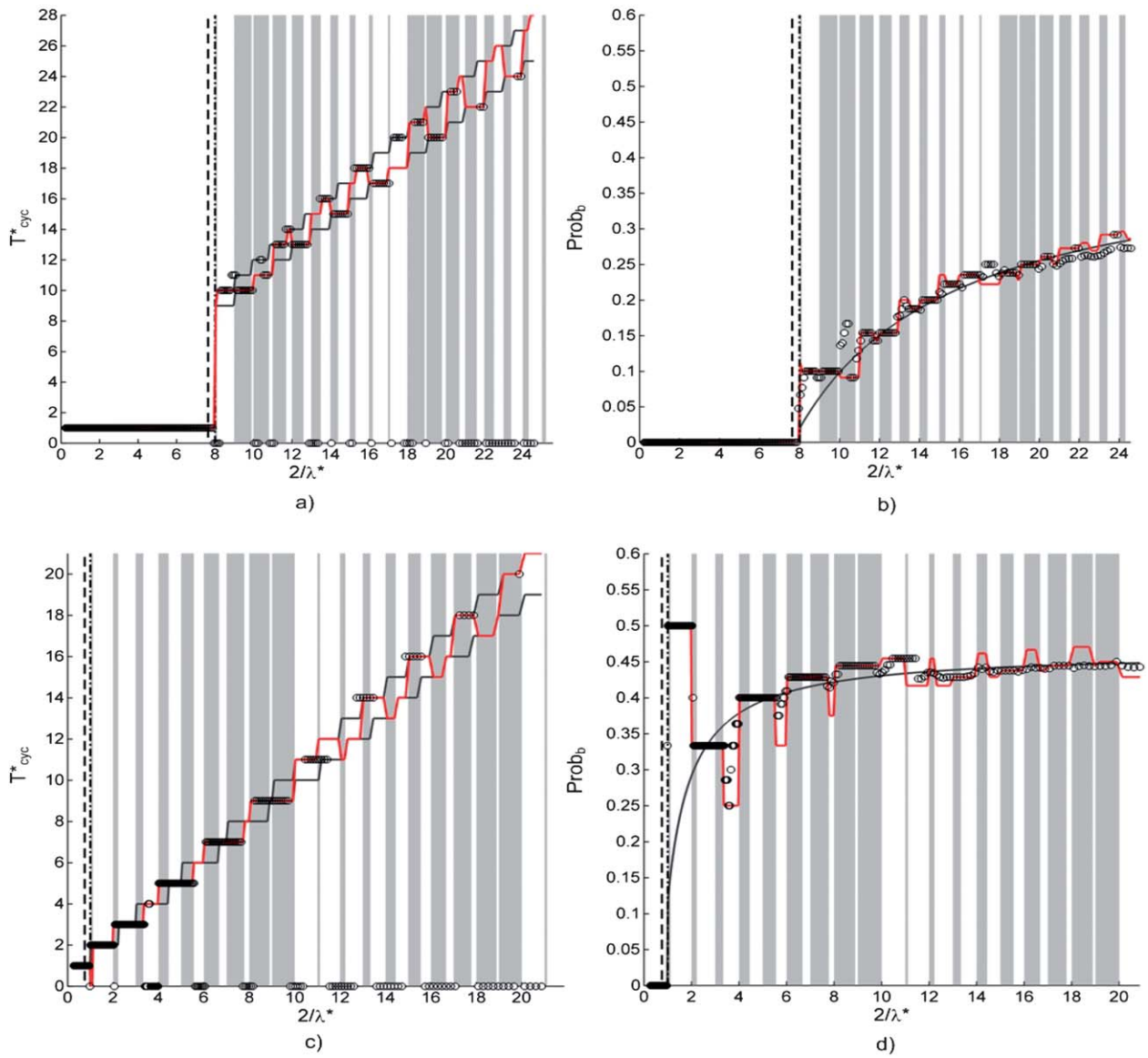

Fig. 3 Full-model numerical simulation results for the T^*_{cyc} and P_b for (a and b) $\Lambda^* = 0.8$, $P^* = 1$, $R^{*(a)}_{drop} = 0.05$; (c and d) $\Lambda^* = 0.9$, $P^* = 0.821$, $R^{*(a)}_{drop} = 0.2$. Chaotic results are indicated by markers along the baseline.

Closer inspection of the chaotic regimes reveals that they typically consist of very long patterns that are mostly composed from fragments of the bracketing stable regimes.[1] For example, if the two bracketing regimes are $T^*_{cyc} = 4,5$ with sequences of UDUD and UUUDD, then these may appear in the longer chaotic sequence such as dUUUDDuUDUDudu. This suggests that in the chaotic regimes the system is constantly switching between two potential cycles.

One of the main facets of the discrete model is that the two flow rates are equal on average; this is not true, however, if the sequence does not absolutely balance the two branches. In the case of a symmetric design, odd sequences which are generally chaotic,[1] result in a permanent imbalance in the flow rates since one branch always has more droplets than the other. This in turn results in a deviation in the output spacings of the two branches from the ideal value ($\lambda_{a,b} = \lambda/2$). Thus a hypothesis may be suggested: *a predicted pattern is unstable if one of the cycle times accounting for the flow imbalance is different from the ideal case*. If the flow imbalance is not great enough to cause the cycle time to change, then the pattern is stable, otherwise it is unstable. Below a simple calculation is developed for determining the stability of a pattern based on this hypothesis.

6.1 Stability analysis

The flow imbalance can be estimated from the number of Us and Ds:

$$\varphi^* = \frac{Q_b}{Q_a} = P^* \frac{R^{(a)}_{hyd} + N_U R_{drop}}{\left(R^{(b)}_{hyd} + N_D R_{drop}\right)} \kappa \qquad (20)$$

This calculation is actually an overestimation of the flow imbalance, because the number of droplets in both channels on average is less than N_U and N_D. Calculating the average is not

straightforward because we would need to know the temporal distribution beforehand. Instead, we adjust the calculation using a fitting parameter, $0 < \kappa < 1$, to account for the fact that the true imbalance is less than predicted by eqn (20). The shift in the flow imbalance, φ^*_{sh}, from the ideal case may be calculated as:

$$\varphi^*_{sh} = (\varphi^* - 1)\frac{1}{2} \tag{21}$$

where the distribution of flow in the two branches then becomes:

$$\varphi^*_a = \frac{Q_a}{Q} = 0.5 - \varphi^*_{sh}; \quad \varphi^*_b = \frac{Q_a}{Q} = 0.5 + \varphi^*_{sh} \tag{22}$$

Subsequently, modified cycle times can be predicted because of this adjustment in flow rates: $T^*_{a\ mod} = \text{ceil}(1/\lambda^*\varphi^*_a)$; $T^*_{b\ mod} = \text{ceil}(\Lambda^*/\lambda^*\varphi^*_b)$. Our hypothesis is that a pattern will be chaotic if one of the modified cycle times does not equate to the corresponding ideal cycle time.

Fig. 4 shows the predicted stable and unstable regions for two cases. A red line distinguishes regions that are expected to be stable and a blue line those that are unstable. These two lines are offset from the numerical data to make the comparison clearer. Particularly good agreement is found for the symmetric case (Fig. 4a). The gradual decay of higher ordered odd patterns is accurately captured by the calculation. The prediction of the asymmetric examples (Fig. 4b) is not as good, but still respectable. The poor performance is most likely due to the uniform κ factor used throughout the calculations. In reality the average weighting will not be uniform. Still, the overall qualitative agreement between the prediction and the simulations suggests that the foundation of the hypothesis is correct.

Additional non-idealities in the system, such as stochastic noise present in experiments, contribute to a decrease in the overall stability. The presence of noise is included in the simulations by purposefully adding variance to the incoming droplet spacing. Simulations were run for the completely symmetric design with the inclusion of spacing fluctuations of 1%, 3% and 5.5% standard deviations (σ). Overall the results were qualitatively similar to the original case; however the number and breadth of the chaotic regimes increased proportionally with variance. Similar results were found when the droplet resistance fluctuated. Additional noise contributions can be included in the stability calculation by simply substituting the extreme limits of the variable (*e.g.* 2 times σ) into the calculation of $T^*_{a\ mod}$ and $T^*_{b\ mod}$.

7. Experimental

Details for the experimental methodology are provided in the ESI†. Experiments were performed in PDMS microfluidic chips using high-speed video analysis to track droplet trajectories. The continuous phase was silicone oil and the dispersed phase was water/glycerol (40/60% w/w) with 1% sodium dodecyl sulfate (SDS). To obtain stable patterns extensive care was taken in designing the microfluidic chip and experimental setup which is discussed in detail in the ESI†. In particular, the variations in spacing and droplet size were kept to a minimum (<2%).

Experiments were performed with symmetric (5 : 5 mm) and asymmetric (5 : 4 mm) branch designs with pressure biases as well. Droplets were spaced far apart to eliminate any interaction.[4] Results are presented for two cases, $\Lambda^* = 1$, $P^* = 1$ and $\Lambda^* = 0.8$, $P^* = 0.76$ in Fig. 5, with additional data presented in the ESI†. In the experiments the junction pressure was inferred by calculating the value from a compact model of the fluidic network. From these calculations, an average P^* was used in the discrete model to describe all of the experimental results. An equivalent droplet resistance of 0.45 mm was measured

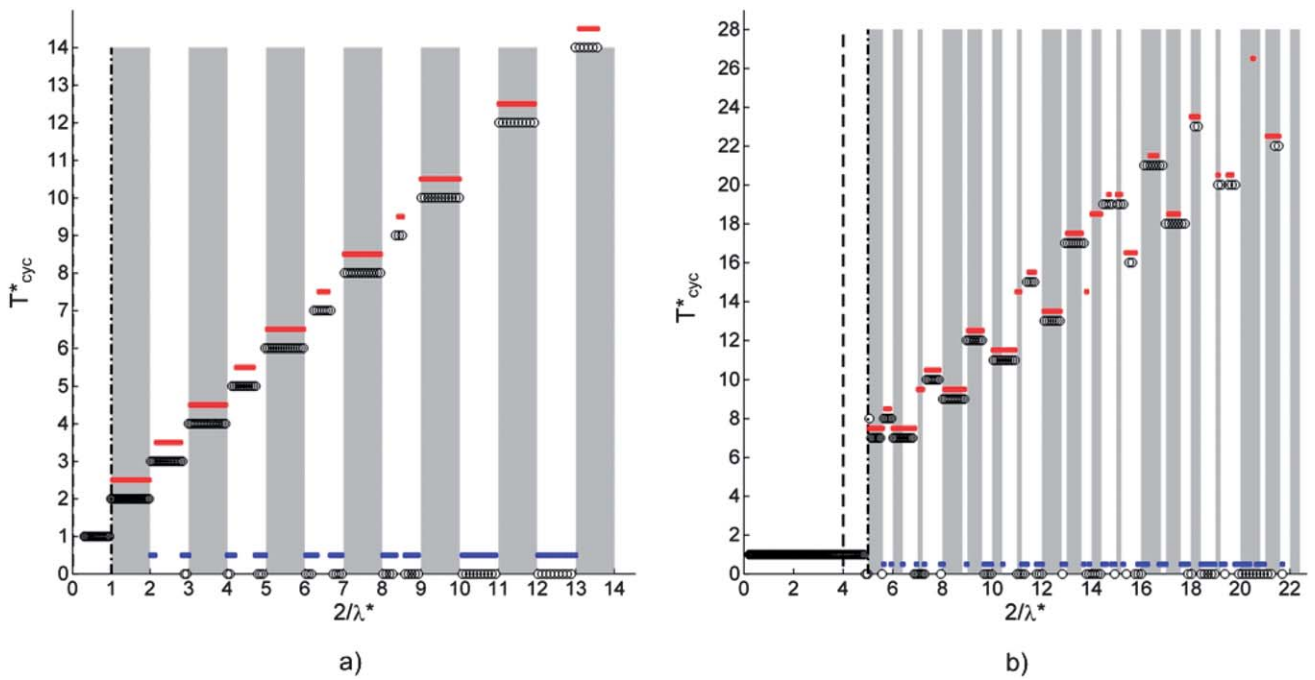

Fig. 4 Full-model numerical simulation results for the T^*_{cyc} with the prediction for stable (red line) and chaotic regimes (blue line). Results are for (a) $\Lambda^* = 1$, $P^* = 1$, $R^{*(a)}_{drop} = 0.1$ and $\kappa = 3/4$ and (b) $\Lambda^* = 0.8$, $P^* = 1$, $R^{*(a)}_{drop} = 0.05$ and $\kappa = 1/3$.

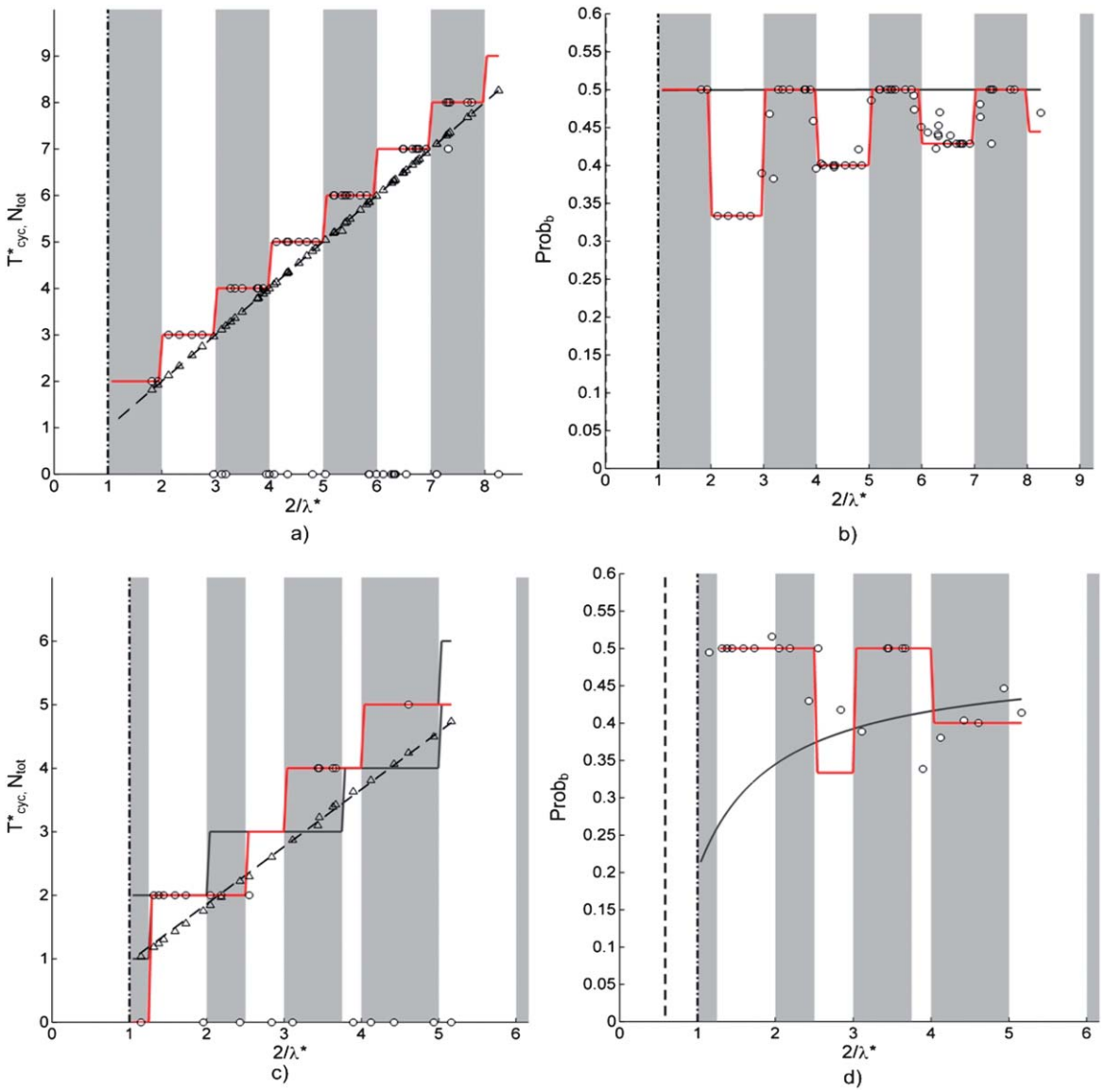

Fig. 5 Experimental results for the T_{cyc} and n_T for (a and b) symmetric branches and pressures $\Lambda^* = 1$, $P^* = 1$ and (c and d) asymmetric branches and asymmetric pressures $\Lambda^* = 0.8$, $P^* = 0.76$. Dashed line in (a and c) (–) is the continuum model prediction for the total number of droplets and Δ the experimental measurement.

independently and used in the calculations (refer to the ESI†). Droplet speeds typically ranged from 2 to 5 mm s^{-1} (equivalent to Ca = 0.002) and the droplet length consistently around 1.5 times the width of the channel.

Many of the same features that appear in the numerical simulations are visible in the experimental results. Filtering cut off, cycling times, total number of droplets and droplet distribution are all well predicted by the models. Both regular and chaotic periodic regimes were obtained across the full spectrum, though there is a noticeable decrease in the size and number of stable periodic regimes as compared to the full-numerical simulations; the reason being the presence of additional non-idealities in the real physical system.[1] Repeating patterns as large as 8 droplets were observed for the completely symmetric case including all possible unique sequences. Overall we see good qualitative and quantitative agreement between the experimental results and the predictions from the continuum and discrete models.

8. Practical implications

The obvious practical application of the sorting phenomena is to use it to split the population of droplets into two groups. Adjusting the pressure bias between the branches allows for control over the distribution of droplets. Here a few comments are made on the practical implementation of such a sorting module in a larger network design along with a few general design rules that have come to light from this study.

There are two possible designs, the first with the intention of sorting specific droplets out of population, say the 3rd and 5th droplet out of every 7, and the second with the intention of sampling a fraction (2/7^{ths}) of the droplets at random. The former

is very difficult to achieve in practice. Even if the best care is taken when designing and operating the chip, it is still difficult to realize stable sorting as evidenced in this study and others.[1,2,14] Furthermore, choosing only the 3rd and 5th droplet would require that a specific sequence needs to repeat *ad infinitum* (*i.e.* UUDUDUU). We know, however that not all sequences are probably available at a given spacing and that the specific sequence that forms depends on the initial conditions which are difficult to control. One option would be to create a severe disturbance to switch the system between sorting patterns.[1] The different patterns can be cycled through until the right one is reached. This of course will take some time and many droplets will sort to the wrong channel before the system is set up.

The design of a "*random droplet sampler*" is more straightforward. The goal should be to run the sorter in one of the chaotic regimes where no specific pattern exists. Generally, it seems best to operate the system at high $2/\lambda^*$ since the system is more likely to be chaotic. At low $2/\lambda^*$ the distribution of droplets is discontinuous since only a fixed set of plateaus can be reached due to pattern formation. At high $2/\lambda^*$ the function is more continuous allowing for a wider range of potential distributions. Additionally, in this high range, the distribution of droplets is closely approximated by the much simpler continuum model. To avoid the chance of a pattern forming small disturbances can be added to the system such as oscillating the outlet pressures slightly or purposefully varying the incoming spacing around an average value. The full-model simulations indicate that generally the system follows the continuum model when $2/\lambda^* > 20$. Therefore, for a typical droplet spacing of 1 mm the corresponding branch length is 10 mm. This is a reasonable size that can fit into most chip designs.

9. Conclusion

We have presented a detailed analysis of droplet sorting at a simple junction with various degrees of asymmetry in the geometry and flow conditions. Using the compact numerical modelling we were able to develop a discrete model of the system that predicts several features including transitions between filtering and sorting, bifurcation in the patterns, composition of the patterns, and estimates of the stability of a pattern. The non-trivial dependence on the various factors was well captured by our model in both numerical and experimental case studies. The complexity of flow produced from a simple junction emphasizes the challenge that remains for the design of large-scale automated droplet networks.

Acknowledgements

The authors gratefully acknowledge the support from the Natural Sciences and Engineering Research Council of Canada for research grants to CR and research support to CE, and the Canada Graduate Scholarship to TG.

Notes and references

1 O. Cybulski and P. Garstecki, *Lab Chip*, 2010, **10**, 484–493.
2 D. A. Sessoms and A. Amon, *et al.*, *Phys. Rev. Lett.*, 2010, **105**, 154501.
3 B. J. Smith and D. P. Gaver, *Lab Chip*, 2010, **10**, 303–312.
4 V. Labrot and M. Schindler, *et al.,* Biomicrofluidics*, 2009, 012804.*
5 S. A. Vanapalli and A. G. Banpurkar, *et al.,* Lab Chip*, 2009, **9**, 982–990.*
6 M. J. Fuerstman and A. Lai, *et al.,* Lab Chip*, 2007, 7, 1479–1489.*
7 K. Nagel, *Phys. Rev. E: Stat. Phys., Plasmas, Fluids, Relat. Interdiscip. Top.*, 1996, **53**, 4655–4672.
8 R. T. Carr and M. Lacoin, *Ann. Biomed. Eng.*, 2000, **28**, 641–652.
9 D. Angeli and J. E. Ferrell, *et al.*, *Proc. Natl. Acad. Sci. U. S. A.*, 2004, **101**, 1822–1827.
10 M. Prakash and N. Gershenfeld, *Science*, 2007, **315**, 832–835.
11 L. F. Cheow and L. Yobas, *et al.*, *Appl. Phys. Lett.*, 2007, **90**, 054107.
12 M. D. Behzad and H. Seyed-allaei, *et al.*, *Phys. Rev. E: Stat., Nonlinear, Soft Matter Phys.*, 2010, **82**, 037303.
13 M. J. Fuerstman and P. Garstecki, *et al.*, *Science*, 2007, **315**, 828–832.
14 G. Cristobal and J. P. Benoit, *et al.*, *Appl. Phys. Lett.*, 2006, **89**, 034104.
15 M. Yamada and S. Doi, *et al.*, *J. Colloid Interface Sci.*, 2008, **321**, 401–407.
16 X. Niu and S. Gulati, *et al.*, *Lab Chip*, 2008, **8**, 1837–1841.
17 H. Boukellal and S. Selimovic, *et al.*, *Lab Chip*, 2009, **9**, 331–338.
18 C. N. Baroud and F. Gallaire, *et al.*, *Lab Chip*, 2010, **10**, 2032–2045.
19 S. Y. Teh and R. Lin, *et al.*, *Lab Chip*, 2008, **8**, 198–220.
20 L. Shui and J. C. T. Eijkel, *et al.*, *Adv. Colloid Interface Sci.*, 2007, **133**, 35–49.
21 D. R. Link and S. L. Anna, *et al.*, *Phys. Rev. Lett.*, 2004, **92**, 054503.
22 Y. C. Tan and Y. L. Ho, *et al.*, *Microfluid. Nanofluid.*, 2008, **4**, 343–348.
23 M. Belloul and W. Engl, *et al.*, *Phys. Rev. Lett.*, 2009, **102**, 194502.
24 W. Engl and M. Roche, *et al.*, *Phys. Rev. Lett.*, 2005, **95**, 208304.
25 D. A. Sessoms and M. Belloul, *et al.*, *Phys. Rev. E: Stat., Nonlinear, Soft Matter Phys.*, 2009, 80.
26 F. Jousse and R. Farr, *et al.*, *Phys. Rev. E: Stat., Nonlinear, Soft Matter Phys.*, 2006, **74**, 036311.
27 Y. F. Yap and S. H. Tan, *et al.*, *J. Phys. D: Appl. Phys.*, 2009, **42**, 065503.
28 M. Schindler and A. Ajdari, *Phys. Rev. Lett.*, 2008, **100**, 044501.
29 A. M. Leshansky and L. M. Pismen, *Phys. Fluids*, 2009, **21**, 023303.
30 M. C. Jullien and M. Ching, *et al.*, *Phys. Fluids*, 2009, **21**, 072001.
31 H. Bruus, *Theoretical Microfluidics*, Oxford University Press, New York, 2007.
32 J. M. Harris, *Combinatorics and Graph Theory*, Springer, New York, 2008.

